Chinese Chemical Letters 35 (2024) 108326

Contents lists available at ScienceDirect

Chinese Chemical Letters

journal homepage: www.elsevier.com/locate/cclet

Selective separation of pyrene from mixed polycyclic aromatic hydrocarbons by a hexahedral metal-organic cage

Ya-Liang Lai, Juan Su, Le-Xiong Wu, Dong Luo, Xue-Zhi Wang, Xian-Chao Zhou, Chuang-Wei Zhou, Xiao-Ping Zhou*, Dan Li

College of Chemistry and Materials Science, Guangdong Provincial Key Laboratory of Functional Supramolecular Coordination Materials and Applications, Jinan University, Guangzhou 510632, China

ARTICLE INFO

Article history:
Received 23 December 2022
Revised 10 February 2023
Accepted 8 March 2023
Available online 11 March 2023

Keywords:
Polycyclic aromatic hydrocarbons
Metal-organic cage
Host-guest chemistry
Selective separation

ABSTRACT

Polycyclic aromatic hydrocarbons (PAHs) play an important role in the industry, and the development of new materials for the selective separation of PAHs is of great significance. In this work, we report a hexahedral metal-organic cage with low symmetry by subcomponent self-assembly. In this cage, the eight Zn^{II} centers adopt an interesting ΛΛ/ΔΔΔΔΔΔ or ΛΛΛΛΛΛ/ΔΔ configuration. This cage with a cavity volume of 520 $Å^3$ can bind anthracene, phenanthrene, and pyrene to form 1:1 host-guest complexes, while the bigger triphenylene, chrysene, perylene, and coronene cannot be encapsulated. The binding constant K_a of pyrene is about 1.110×10^3 $(mol/L)^{-1}$, which is more than an order of magnitude larger than that of anthracene and phenanthrene (111 $(mol/L)^{-1}$, 277 $(mol/L)^{-1}$, respectively). X-ray structure studies reveal that the pyrene is located in the cavity and stabilized by multiple C–H···π interactions. After separation from a mixture of PAHs, pyrene with >96.1% purity can be obtained. This work provides a useful method for the first time for the selective separation of pyrene from PAHs mixture by utilizing a metal-organic cage as the material, making it a useful tool for purifying and separating specific compounds from complex mixtures.

Polycyclic aromatic hydrocarbons (PAHs) are a class of compounds formed by the fusion of two or more benzene rings in a linear, angular, or cluster arrangement [1,2]. Pyrene, one of the important components of PAHs, has been widely used in various areas due to its rigid structure, excellent fluorescence properties, and electron-rich conjugation properties [3–6]. In industry, pyrene is mainly derived from the destructive distillation of coal tar, and the separation and purification process usually consumes huge energy. Therefore, it is emergent to develop new technologies for the selective separation of pyrene from the mixture of PAHs with high efficiency.

Metal-organic frameworks (MOFs) are crystalline porous materials with framework structures, which are formed by the self-assembly of organic ligands and metal ions through coordination bonds [7,8]. In contrast to MOFs, metal-organic cages (MOCs) are molecular materials with isolated cage-like structures, which are also constructed by metal ions and organic ligands [9,10]. However, most of the MOCs have good solvent solubility [11–13], and can be characterized by the methods utilized in traditional solution chemistry and used as molecular materials in solution state for application in separation [14–18], catalysis [19–21], chiral recognition [22,23], fluorescence sensing [24,25], stabilization of active substances [26,27] and drug delivery [28,29]. Due to their rich structures with tunable cavities, MOCs can effectively bind PAHs through weak interactions (*e.g.*, π-π stacking and C–H···π interactions) in solution [30,31]. Although many MOCs can encapsulate the PAHs, the limited examples that can specifically recognize PAHs to achieve selective separation have been reported [17,32,33]. Recently, Mukherjee *et al.* reported a water-stable $[Pd_4L_2]^{8+}$ molecular vessel capable of selectively separating phenanthrene from a mixture of anthracene and phenanthrene in water [33]. Nitschke *et al.* reported the selective encapsulation and separation of coronene from a mixture of PAHs *via* phase transfer of a tetrahedral MOC [32]. In addition, some MOFs have also been used as materials for the separation of PAHs [34,35]. However, to the best of our knowledge, the selective separation of pyrene from PAHs has not yet been achieved by using MOCs or MOFs as separating materials.

Herein, we report a hexahedral metal-organic cage, formulated as $[(Zn^{II}_8L_6)(OTf)_{16}]$ (denoted as **1**, Scheme 1), which is constructed by subcomponent self-assembly of TAPB (1,2,4,5-tetrakis-(4-aminolphenyl)benzene), 2-formylpyridine, and $Zn(OTf)_2$.

* Corresponding author.
E-mail address: zhouxp@jnu.edu.cn (X.-P. Zhou).

https://doi.org/10.1016/j.cclet.2023.108326
1001-8417/

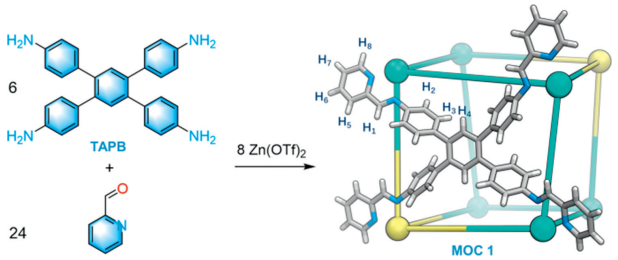

Scheme 1. Schematic diagram of self-assembly of MOC **1.**

In cage **1**, the eight Zn^{II} centers adopt unusual ΛΛ/ΔΔΔΔΔΔ or ΛΛΛΛΛΛ/ΔΔ configuration, which leads to low symmetry for a hexahedron [36]. Cage **1** contains an electron-rich hydrophobic inner cavity with a volume of 520 $Å^3$, which can act as a potential host for PAHs. We selected seven PAHs (anthracene, phenanthrene, pyrene, triphenylene, chrysene, perylene, and coronene) to study their host-guest chemistry due to the suitable free molecular volumes (ranging of 262–392 $Å^3$). Interestingly, MOC **1** can bind anthracene, phenanthrene, and pyrene to form 1:1 host-guest complexes, respectively, while triphenylene, chrysene, perylene, and coronene cannot be encapsulated by **1** due to their big molecular volumes. Moreover, MOC **1** shows the best affinity to pyrene. The binding constant K_a is about 1.110×10^3 $(mol/L)^{-1}$, which is more than an order of magnitude larger than for anthracene and phenanthrene (111 $(mol/L)^{-1}$, 277 $(mol/L)^{-1}$, respectively). X-ray structure of the host-guest complex pyrene⊂**1** display that the pyrene is located in the cavity and stabilized by multi C–H$\cdots\pi$ interactions. Further studies showed that MOC **1** could selectively encapsulate pyrene from a mixture of seven PAHs. The pyrene with 96.1% purity can be obtained by a separation cycle. For the first time, the selective separation of pyrene from the PAHs mixture is achieved by the design of MOC with a suitable cavity.

TAPB was synthesized by following a reported procedure (see experimental section in Supporting information for details) [37]. The reaction of TAPB, 2-formylpyridine, and $Zn(OTf)_2$ in a 6:24:8 molar ratio in CH_3CN solution at 70 °C for 8 h afforded MOC **1** (Scheme 1). MOC **1** was characterized by nuclear magnetic resonance (NMR), electrospray ionization time-of-flight mass spectrometry (ESI-TOF-MS), thermal gravimetric analyzer (TGA), N_2 adsorption, powder X-ray diffraction (PXRD), and single-crystal X-ray diffraction (SCXRD).

The ^1H NMR spectrum of MOC **1** in CD_3CN displayed three distinct ligand environments, reflecting the presence of three signals on the imine (H_1) and phenyl (H_2, H_3, H_4, Fig. 1a). There exist three sets of signals in the NMR spectrum of **1**, which may be due to the configurational difference of the eight Zn^{II} vertices leading to a low symmetric structure. The ^1H–^1H correlation spectroscopy (COSY) data also supported this result (Fig. S3 in Supporting information). Two-dimensional (2D) ^1H–^1H diffusion-ordered spectroscopy (DOSY) studies showed that the ^1H signals of MOC **1** in CD_3CN mainly belonged to a single species with a log*D* of about −9.38 (Fig. 1a). The hydrodynamic radius was calculated to be ~14.9 Å *via* the Stokes-Einstein equation [38].

Mass spectrometry is a powerful method to study the structure of supramolecular cages [39]. The composition of MOC **1** was precisely determined by ESI-TOF-MS in CH_3CN. The most prominent peak at $m/z = 951.1409$ was corresponding to the [**1**–9OTf]$^{7+}$ (calcd. 951.1399) species. Other signs at $m/z = 813.6223$, 1134.4832, 1391.1659, and 1776.1921 correspond to [**1**–8OTf]$^{8+}$ (calcd. 813.6219), [**1**–10OTf]$^{6+}$ (calcd. 1134.4825), [**1**–11OTf]$^{5+}$ (calcd. 1391.1667), and [**1**–12OTf]$^{4+}$ (calcd. 1776.1924), respectively (Fig. 1b). The experimental isotopic patterns of these peaks closely match their theoretical patterns (Fig. 1b and Fig. S4 in Supporting information), which confirms the $Zn^{II}_8L_6$ composition of MOC **1**. The MS results also manifest that MOC **1** is stable in the CH_3CN solution.

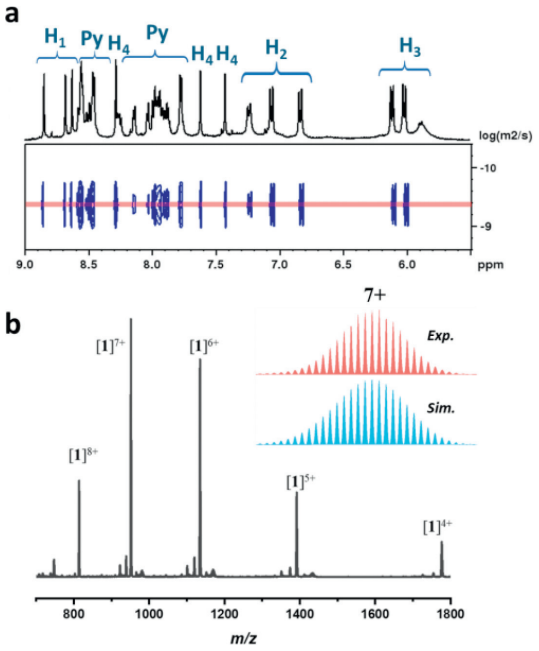

Fig. 1. (a) Partial ^1H NMR and DOSY spectra of MOC **1** in CD_3CN. (b) Mass spectrum of MOC **1** in CH_3CN. Insets show the calculated (blue) and experimental (red) isotopic patterns of the +7 peak at $m/z = 951.1409$ corresponding to the species of [**1**–9OTf]$^{7+}$.

Thermogravimetric analysis (TGA) showed that MOC **1** was stable to about 350 °C (Fig. S5 in Supporting information). Unfortunately, crystals of MOC **1** were not stable in air, and they changed to amorphous after exposure to air due to lost the guest solvent molecules, which was confirmed by PXRD of MOC **1** (Fig. S6 in Supporting information). Such a phenomenon is normal for MOCs. N_2 adsorption experiment was also carried out. The result showed that MOC **1** was not a good porous solid material (Fig. S7 in Supporting information).

Yellow block crystals of MOC **1** suitable for single crystal X-ray diffraction (SCXRD) analysis were obtained by diffusing ethyl acetate vapor into its CH_3CN solution. SCXRD revealed that **1** crystallizes in the space group $P2_1/n$, featuring an 8-nuclear hexahedral cage structure (Fig. 2a). Six ligands as faces bind eight Zn^{II} ions to form the hexahedral cage. Interestingly, the Zn^{II} centers adopt ΛΛΔΔΔΔΔΔ or ΛΛΛΛΛΛΔΔ configurations (Figs. 2c and d), and both two enantiomers co-existed in the crystal structure to produce the racemate **1** (Fig. 2a). Notably, MOC **1** can be reduced to an irregular hexahedral ball-stick structure by treating the Zn^{II} centers as nodes (Fig. 2b). The two ΛΛ or ΔΔ Zn^{II} centers were located on the body diagonal of the hexahedron, which probably lead to the form of a hexahedral cage with a symmetry of D_3. The low symmetry of **1** was consistent with the result of its ^1H NMR in CD_3CN [40]. Although a lot of hexahedral MOCs have been reported [41–43], to the best of our knowledge, such vertex configurations are observed for the first time. The metal-to-metal distances of Zn^{II} centers forming adjacent vertices range from 10.332 Å to 13.601 Å, further suggesting the low symmetry in **1**. The maximum dimension is 28.543 Å (H$\cdots$H distance), which is in good agreement with the results of DOSY. MOC **1** has an electron-rich hydrophobic cavity with a volume of 520 $Å^3$ estimated by VOIDOO [44], which is probably an ideal host for encapsulation and separation of PAHs.

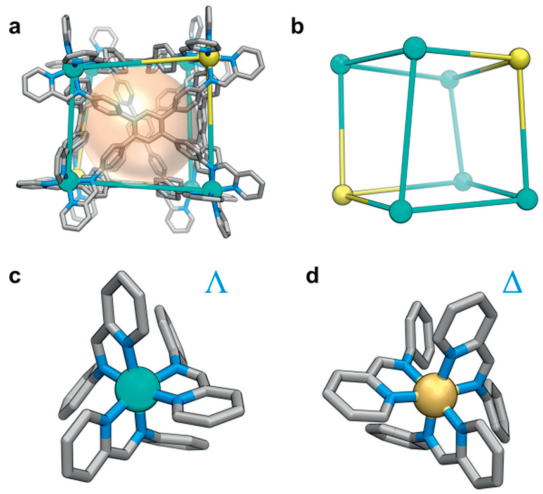

Fig. 2. X-ray Crystal structure of MOC **1**: (a) Hexahedral cage structure, (b) topology structure, and coordination in (c) Λ and (d) Δ absolute configurations for octahedral zinc centers. The Zn^{II} centers with Δ and Λ configurations were colored orange-yellow and cyan, respectively. gray, C; blue, N. The anions and hydrogen atoms were omitted for clarity.

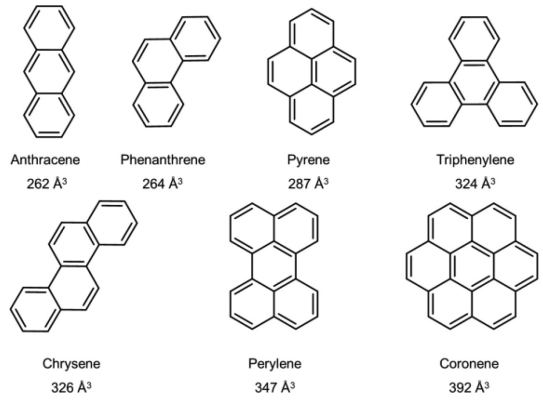

Fig. 3. PAH molecules and their volumes. Materials Studio 2018 was used for the calculation. The Connolly radius vdW, scale factor, and grid interval were set as 1.0 Å, 1.26 and 0.7 Å, respectively.

As shown in Fig. 3, seven PAHs were chosen to study the host-guest chemistry with MOC **1**. Before the experimental study, we calculated their molecular volume by using Materials Studio 2018. The free volumes of PAHs were generated by using the accessible Connolly surface calculation. As shown in Fig. 3, the molecular volumes of these PAHs range from 262 $Å^3$ to 392 $Å^3$ and are smaller than the volume of **1** (520 $Å^3$). Interestingly, the molecular volume of pyrene is 287 $Å^3$, and its packing coefficient (ratio of guest volume to host volume) in the cavity of **1** will be 55.2%. According to Rebek's rule [30,45,46], the best binding will be reached for pyrene. In addition, the two-dimensional sizes of these seven PAH molecules were also calculated (Table S2 in Supporting information). The range of the minimum size of each molecule was 7.388–11.901 Å, which is smaller than the maximum cavity size of the cage (Zn-Zn distances, 13.601 Å), suggesting that **1** can probably trap these PAHs.

Based on the above theoretical calculation results, the experiments of host-guest chemistry of MOC **1** and PAHs (Fig. 3) were carried out. In a typical experiment, the MOC **1** was dissolved in CD_3CN or CD_3NO_2 (0.6 mL, 0.002 mmol), and excess PAHs were added, respectively. The solution was equilibrated at 60 °C for 3 h, and the reactants were characterized by ^1H NMR.

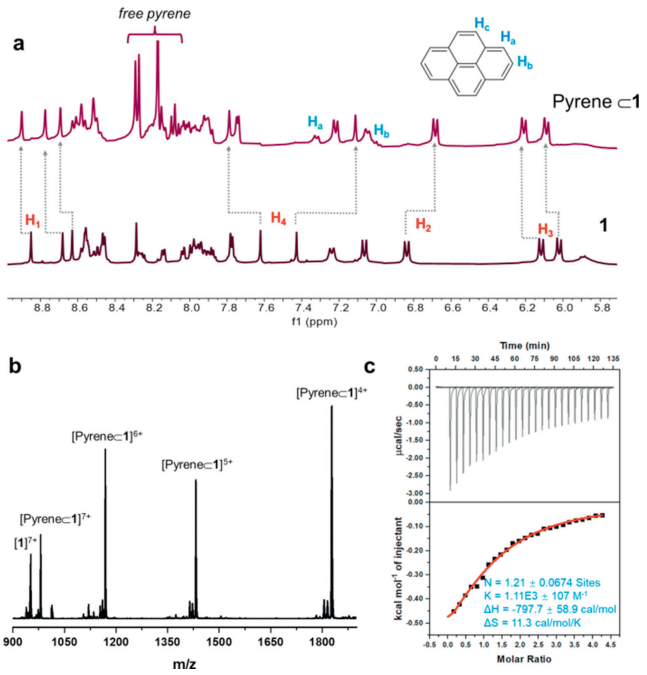

Fig. 4. (a) Aromatic region of the ^1H NMR spectra of free **1** (bottom), and pyrene⊂**1** formed by adding 5 equiv. of pyrene to **1** (top). (b) Mass spectrometry of pyrene⊂**1**. (c) Binding isotherm corresponding to the ITC titration of **1** with pyrene ([**1**] = 1.0 mmol/L, and [pyrene] = 20.0 mmol/L, CH_3CN/CH_3OH (v/v = 1:1) at 30 °C).

As shown in Fig. 4, the ^1H NMR peaks of **1** showed significant downfield or upfield shifting in comparison to the free **1** were observed for the imine (H_1, $|\Delta\delta| = 0.05–0.10$ ppm) and phenyl protons (H_2 $|\Delta\delta| = 0.16$ ppm, H_3 $|\Delta\delta| = 0.07–0.09$ ppm, H_4 $|\Delta\delta| = 0.16–0.51$ ppm) after encapsulation of pyrene. In addition, two peaks (H_a, H_b) of the bound pyrene were observed in the spectrum of pyrene⊂**1** (Fig. 4a, Figs. S8 and S9 in Supporting information). The unidentified signal of Hc was probably overlapped with the signals of the MOC **1**. The $^1H–^1H$ COSY spectrum showed a strong correlation between H_a and H_b, suggesting that H_a and H_b belong to the encapsulation of pyrene. The obvious upfield shift of H_a, H_b in comparison to the signs of free pyrene (about 1.0 ppm), suggests that host **1** exhibits a slow-exchange binding process on the proton NMR timescale. The host-guest stoichiometry was found to be 1:1 by integration of the peaks of ^1H NMR of pyrene⊂**1**, suggesting that one cage molecule can host a pyrene molecule. This result is consistent with the packing coefficient (55.2%).

ESI-TOF-MS was further employed to confirm the formation of pyrene⊂**1**. As shown in Fig. 4b and Fig. S10 (Supporting information), the peaks with *m/z* values of 980.1313, 1168.3345, 1431.7878 and 1827.0033 correspond to $[pyrene⊂\mathbf{1}–9OTf]^{7+}$ (calcd. 980.1421), $[pyrene⊂\mathbf{1}–10OTf]^{6+}$ (calcd. 1168.3278), $[pyrene⊂\mathbf{1}–11OTf]^{5+}$(calcd. 1431.7202), and $[pyrene⊂\mathbf{1}–12OTf]^{4+}$ (calcd. 1826.9314), respectively. This result further manifests that MOC **1** successfully encapsulated the pyrene as the guest with a 1:1 stoichiometric ratio.

We also tested other six PAHs. Similar to pyrene, both anthracene and phenanthrene can also be encapsulated by MOC **1** successfully, respectively, which were documented by ^1H NMR and ESI-TOF-MS studies (Figs. S11-S14 in Supporting information). Due to the poor solubility of these PAHs in CD_3CN, the encapsulating reactions with MOC **1** were carried out in CD_3NO_2. As shown in Figs. S15-S18 (Supporting information), the ^1H NMR peaks of **1** were not shifted after adding the triphenylene, chrysene, perylene, and coronene into its CD_3NO_2 solution, respectively. As a comparison, we tested the encapsulating experiment of pyrene in CD_3NO_2. The results showed that pyrene was successfully encapsulated by **1**

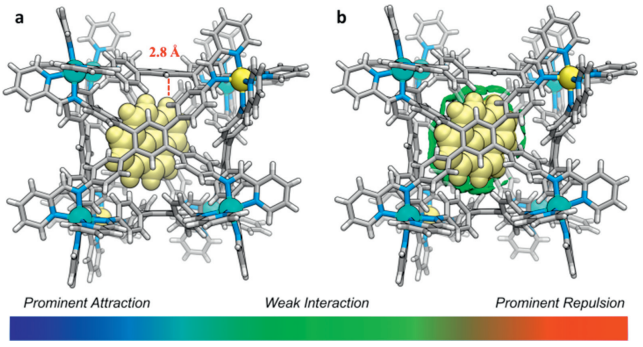

Fig. 5. (a) Crystal structure of pyrene⊂**1** (C–H···π interactions were highlighted with a dashed red line). (b) Independent gradient model for the Hirshfeld partition (IGMH) analysis between pyrene and the wall of the cavity in **1**. The color scale showed a range of interaction strengths: prominent attraction (blue), weak interaction (green), and prominent repulsion (red). The anions and ethyl acetate were omitted for clarity. Color labels: Zn, cyan or yellow; C, gray; N, blue; H, light gray. Pyrene was shown as a space-filling mode with yellow color.

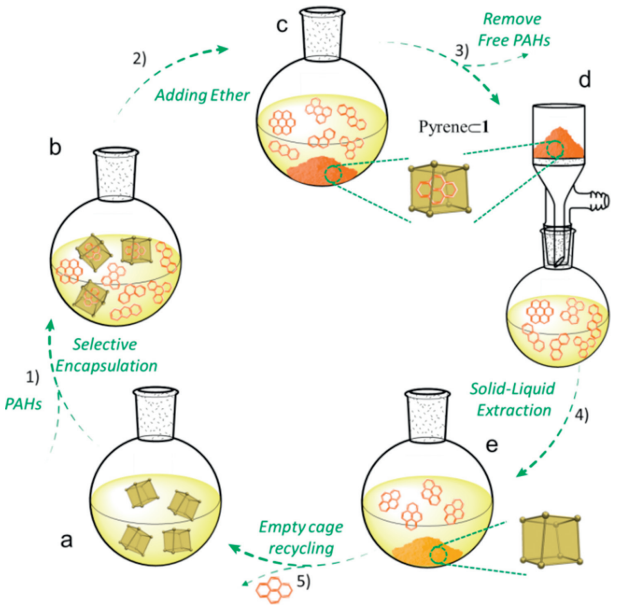

Fig. 6. Selective separation and extraction of pyrene from PAHs mixtures: (a) **1** was dissolved in CH_3CN and (b) selectively encapsulated pyrene to form pyrene⊂**1**. (c) Pyrene⊂**1** was precipitated, and the free PAHs were dissolved in a mixed solvent of ether and CH_3CN. (d) The powder of pyrene⊂**1** was obtained by filter. (e) The bound pyrene was released by solid-liquid extraction with ethyl acetate to obtain empty **1** and pure pyrene.

(Fig. S19 in Supporting information). These results indicate that the triphenylene, chrysene, perylene, and coronene cannot be bound by MOC **1**, which is probably due to their relatively bigger molecular volumes (Fig. 3).

According to the reported procedure [32], the binding constants of pyrene, anthracene, and phenanthrene to MOC **1** were determined by ^{1}H NMR integration at 298 K. The binding constants K_a for anthracene, phenanthrene, and pyrene were estimated to be approximately 111 $(mol/L)^{-1}$, 277 $(mol/L)^{-1}$ and 1184 $(mol/L)^{-1}$, respectively. Furthermore, isothermal titration calorimetry (ITC) was employed to measure the binding constants, which was often used to study the host-guest chemistry of coordination cages [47,48]. As shown in Fig. 4c, upon the addition of pyrene (20.0 mmol/L) to a CH_3CN/CH_3OH (v/v = 1:1) solution of **1** (1.0 mmol/L) yielded association constants of 1110 ± 107 $(mol/L)^{-1}$, the titration fit curve showed the molar ratio of 1:1 for the host-guest complex. The results of ITC were in good agreement with the results obtained by ^{1}H NMR and mass spectrometry. The ΔH and ΔS values were −797.7 cal/mol and 11.3 cal mol^{-1} K^{-1}, respectively, indicating that the complexation reaction was driven by enthalpy. The titration results showed no obvious heat change was observed by adding anthracene and phenanthrene into the CH_3CN/CH_3OH solution of **1** under the same conditions (Fig. S20 in Supporting information), respectively. These results indicated that the binding between anthracene (or phenanthrene) and MOC **1** was very weak, which is consistent with their small binding constants obtained by ^{1}H NMR.

To understand the mechanism of the encapsulation, we attempt to obtain the crystal structure of pyrene⊂**1**. Excess of pyrene was added to the CH_3CN solution of MOC **1** and slowly diffused with ethyl acetate vapor, the crystals of pyrene⊂**1** suitable for X-ray diffraction analysis were obtained after about 1 week. As shown in Fig. 5a, the crystal structure clearly shows that one pyrene molecules locate in the cavity of **1**. The shortest distance between the pyrene and **1** was about 2.8 Å (C···H distance), which indicates that there exist C–H···π interactions in them. After the encapsulation of pyrene, the metal-metal distances of the adjacent vertex Zn^{II} center range from 10.336 Å to 13.666 Å, which were very close to that of guest free **1**, indicating that its cavity volume did not change after encapsulation of pyrene. Interestingly, after encapsulation of pyrene, MOC **1** can further bind ethyl acetate molecules (Fig. S21 in Supporting information). In addition, the independent gradient model of this structural model based on Hirshfeld partitioning (IGMH) [49] analysis showed that the pyrene molecule was surrounded by green isosurfaces (Fig. 5b), and the calculated binding energy was −34.68 kcal/mol. These results indicate that there exist weak interactions between pyrene and the cavity of **1**, which probably stabilize the host-guest complex of pyrene⊂**1**.

The above experimental results suggest that MOC **1** has a stronger capacity in binding pyrene than other PAHs, which may be used as a material for the selective separation of pyrene from the mixture of PAHs. A mixture of PAHs (pyrene, 3 equiv., and other PAHs, 1 equiv., based on **1**) was added to a CH_3CN solution of **1** (20 mL, 0.001 mol/L, Figs. 6a and b). After equilibration at 60 °C for 3 h, the free PAHs were removed by the filter after adding ether, in which the free PAHs were dissolved in the ether and pyrene⊂**1** was precipitated. The powder of pyrene⊂**1** was obtained by filter (Figs. 6c and d). ^{1}H NMR demonstrated the pyrene was mainly selected by **1** to form pyrene⊂**1**, and no ^{1}H NMR signal of other PAH molecules was detected (Fig. S22b in Supporting information). These experimental results indicated that **1** selectively captured the pyrene from the mixture of PAHs. The trapped pyrene can be released by solid-liquid extraction by using ethyl acetate as the solution to obtain the empty **1** (Fig. 6e and Fig. S22c in Supporting information). The successfully recovered pyrene from the mixture was also proved by the ^{1}H NMR spectrum, which showed that the recovered sample contain pyrene with high purity (>98%, Fig. S23 in Supporting information). The high purity of recovered pyrene was further confirmed by high performance liquid chromatography (HPLC), and a purity of 96.1% was determined (Fig. S24 in Supporting information). The separation experiment was performed when pyrene was present in an equal amount in the mixture of PAHs. The results showed that MOC **1** was able to separate pyrene with >90.9% purity (Fig. S25 in Supporting information). In addition, ethyl acetate as a guest molecule bound to the cage does not affect the separation performance. Similar results can be obtained when other poor solvents (ether, toluene, *etc.*) were used for separation experiments. Moreover, the recovered **1** can be further used to separate the pyrene from the mixture. Cage **1** was stable after repeating the separation three times (Fig. S22d in Supporting information), suggesting that **1** was a robust material for the selective separation of pyrene from the PAHs mixture.

In summary, we have designed and synthesized a low symmetric hexahedral metal-organic cage with a cavity volume of 520 Å by subcomponent self-assembly. In MOC **1**, zinc centers display ΛΛ/ΔΔΔΔΔΔ and ΛΛΛΛΛΛ/ΔΔ configurations in its crystal structure, which is discovered in hexahedral MOCs for the first time. The molecular volume of pyrene matches well with the cavity volume of cage **1** (55.2% packing coefficient). Cage **1** has a high affinity to pyrene and can selectively separate pyrene from a mixture of PAHs with high purity. X-ray structure of pyrene⊂**1** showed there exist multi CH$\cdots\pi$ interactions between them, which stabilize the host-guest complex. Moreover, cage **1** is robust and recyclable, providing an advanced material for the selective separation of pyrene from the PAHs mixture. This study provides a new strategy for designing materials based on metal-organic cages for the separation of PAHs, which will probably pave the way for developing new technologies in separation.

Declaration of competing interest

The authors declare that they have no known competing financial interests or personal relationships that could have appeared to influence the work reported in this paper.

Acknowledgments

This work was financially supported by the National Natural Science Foundation of China (Nos. 22171106, 21731002, 21975104, 21871172 and 22201101), the Guangdong Major Project of Basic and Applied Research (No. 2019B030302009), Guangdong Natural Science Foundation (No. 2022A1515011937), the Guangzhou Science and Technology Program (No. 202002030411), the Fundamental Research Funds for the Central Universities (No. 21622103), the China Postdoctoral Science Foundation (No. 2022M711327), and Jinan University.

Supplementary materials

Supplementary material associated with this article can be found, in the online version, at doi:10.1016/j.cclet.2023.108326.

References

[1] V. Kumar, N.C. Kothiyal, et al., J. Chin. Adv. Mater. Soc. 4 (2016) 302–321.
[2] I.J. Keyte, R.M. Harrison, G. Lammel, Chem. Soc. Rev. 42 (2013) 9333–9391.
[3] F.P. Kinik, A. Ortega-Guerrero, D. Ongari, et al., Chem. Soc. Rev. 50 (2021) 3143–3177.
[4] T.M. Figueira-Duarte, K. Müllen, Chem. Rev. 111 (2011) 7260–7314.
[5] F.M. Winnik, Chem. Rev. 93 (1993) 587–614.
[6] A.J. Howarth, M.B. Majewski, M.O. Wolf, Coord. Chem. Rev. 282-283 (2015) 139–149.
[7] M. Zhao, Y. Huang, Y. Peng, et al., Chem. Soc. Rev. 47 (2018) 6267–6295.
[8] N. Stock, S. Biswas, Chem. Rev. 112 (2012) 933–969.
[9] E.S.M. El-Sayed, Y.D. Yuan, D. Zhao, et al., Acc. Chem. Res. 55 (2022) 1546–1560.
[10] S. Daliran, A.R. Oveisi, Y. Peng, et al., Chem. Soc. Rev. 51 (2022) 7810–7882.
[11] T.R. Cook, P.J. Stang, Chem. Rev. 115 (2015) 7001–7045.
[12] A.J. Gosselin, C.A. Rowland, E.D. Bloch, Chem. Rev. 120 (2020) 8987–9014.
[13] L.J. Wang, X. Li, S. Bai, et al., J. Am. Chem. Soc. 142 (2020) 2524–2531.
[14] L.J. Wang, S. Bai, Y.F. Han, J. Am. Chem. Soc. 144 (2022) 16191–16198.
[15] D. Zhang, T.K. Ronson, Y.-Q. Zou, et al., Nat. Rev. Chem. 5 (2021) 168–182.
[16] C. Zhu, H. Tang, K. Yang, et al., J. Am. Chem. Soc. 143 (2021) 12560–12566.
[17] D. Chakraborty, R. Saha, J.K. Clegg, et al., Chem. Sci. 13 (2022) 11764–11771.
[18] W.Y. Zhang, Y.J. Lin, Y.F. Han, et al., J. Am. Chem. Soc. 138 (2016) 10700–10707.
[19] Y. Fang, J.A. Powell, E. Li, et al., Chem. Soc. Rev. 48 (2019) 4707–4730.
[20] Y. Xue, X. Hang, J. Ding, et al., Coord. Chem. Rev. 430 (2021) 213656.
[21] R.L. Spicer, A.D. Stergiou, T.A. Young, et al., J. Am. Chem. Soc. 142 (2020) 2134–2139.
[22] M. Pan, K. Wu, J.H. Zhang, et al., Coord. Chem. Rev. 378 (2019) 333–349.
[23] W. Xuan, M. Zhang, Y. Liu, et al., J. Am. Chem. Soc. 134 (2012) 6904–6907.
[24] A. Brzechwa-Chodzyńska, W. Drożdż, J. Harrowfield, et al., Coord. Chem. Rev. 434 (2021) 213820.
[25] Z. Zhang, Z. Zhao, L. Wu, et al., J. Am. Chem. Soc. 142 (2020) 2592–2600.
[26] P. Mal, B. Breiner, K. Rissanen, et al., Science 324 (2009) 1697–1699.
[27] S. Hasegawa, S.L. Meichsner, J.J. Holstein, et al., J. Am. Chem. Soc. 143 (2021) 9718–9723.
[28] Y.R. Zheng, K. Suntharalingam, T.C. Johnstone, et al., Chem. Sci. 6 (2015) 1189–1193.
[29] H. Sepehrpour, W. Fu, Y. Sun, et al., J. Am. Chem. Soc. 141 (2019) 14005–14020.
[30] F.J. Rizzuto, L.K.S. von Krbek, J.R. Nitschke, Nat. Rev. Chem. 3 (2019) 204–222.
[31] M. Yamashina, Y. Tanaka, R. Lavendomme, et al., Nature 574 (2019) 511–515.
[32] D. Zhang, T.K. Ronson, R. Lavendomme, et al., J. Am. Chem. Soc. 141 (2019) 18949–18953.
[33] A.B. Sainaba, M. Venkateswarulu, P. Bhandari, et al., J. Am. Chem. Soc. 144 (2022) 7504–7513.
[34] S. Sun, L. Huang, H. Xiao, et al., Talanta 202 (2019) 145–151.
[35] M. Tabatabaii, M. Khajeh, A.R. Oveisi, et al., ACS Omega 5 (2020) 12202–12209.
[36] C.T. McTernan, J.A. Davies, J.R. Nitschke, Chem. Rev. 122 (2022) 10393–10437.
[37] H.L. Nguyen, C. Gropp, Y. Ma, et al., J. Am. Chem. Soc. 142 (2020) 20335–20339.
[38] J.T. Edward, J. Chem. Educ. 47 (1970) 261.
[39] H. Wang, C. Guo, X. Li, CCS Chem. 4 (2022) 785–808.
[40] W. Meng, J.K. Clegg, J.D. Thoburn, et al., J. Am. Chem. Soc. 133 (2011) 13652–13660.
[41] J. Jiao, Z. Li, Z. Qiao, et al., Nat. Commun. 9 (2018) 4423.
[42] D. Luo, L.X. Wu, Y. Zhang, et al., Sci. China Chem. 65 (2022) 1105–1111.
[43] W. Meng, B. Breiner, K. Rissanen, et al., Angew. Chem. Int. Ed. 50 (2011) 3479–3483.
[44] G.J. Kleywegt, T.A. Jones, Acta Crystallogr. Sect. D 50 (1994) 178–185.
[45] P. Mal, D. Schultz, K. Beyeh, et al., Angew. Chem. Int. Ed. 47 (2008) 8297–8301.
[46] S. Mecozzi, J. Rebek, Julius, Chem. Eur. J. 4 (1998) 1016–1022.
[47] T. Feng, X. Li, J. Wu, et al., Chin. Chem. Lett. 31 (2020) 95–98.
[48] B.S. Pilgrim, N.R. Champness, ChemPlusChem 85 (2020) 1842–1856.
[49] T. Lu, Q. Chen, J. Comput. Chem. 43 (2022) 539–555.